Supporting Information

Bandgap Tunable Transparent Perovskite Solar Cells for 4T Si/perovskite Tandem Photovoltaics with PCE > 30% via Rational Interface Management

Abhijit Singha,[1†] Tiankai Zhang,[2†] Ananta Paul,[3] M. M. Anas,[4] Karthik Raitani,[5] Manas Misra,[5] Subir Manna,[5] Vishnu Kumar,[5] Sudhanshu Mallick,[3] K. R. Balasubramaniam,[1] Pradeep R. Nair,[4*] Feng Gao,[2*] Dinesh Kabra[5*]

† Contributed equally to this work.

[1]Department of Energy Science and Engineering, Indian Institute of Technology Bombay, Mumbai, 400076, India
[2]Department of Physics, Chemistry and Biology (IFM), Linkoping University, Linkoping, 58183, Sweden
[3]Department of Metallurgical Engineering and Material Science, Indian Institute of Technology Bombay, Mumbai, 400076, India
[4]Department of Electrical Engineering, Indian Institute of Technology Bombay, Powai, Mumbai 400076,India.
[5]Department of Physics, Indian Institute of Technology Bombay, Powai, Mumbai 400076, India.

*Corresponding authors – prnair@ee.iitb.ac.in, feng.gao@liu.se, dkabra@iitb.ac.in

This file includes:

Materials:

Formamidinium iodide (FAI) and methylammonium bromide (MABr) are procured from Great Cell Solar (Australia). Lead iodide (PbI_2), cesium iodide (CsI), and lead bromide ($PbBr_2$) are obtained from TCI. Spiro-OMeTAD (99.8%) is sourced from Lumtec. N,N-dimethylformamide (DMF), dimethyl sulfoxide (DMSO), 4-tert-butylpyridine (t-BP), isopropanol (IPA), chlorobenzene (CB), acetonitrile (ACN), 1,1,2,2-tetrachloroethane (TCE), tin(IV) chloride pentahydrate ($SnCl_4 \cdot 5H_2O$), Rubidium Iodide (RbI), Rubiduam Choloride (RbCl), Dichloromethane (DCM), and lithium bis(trifluoromethanesulfonyl)imide (Li-TFSI) are obtained from Sigma-Aldrich. A colloidal SnO_2 solution (15 wt% in water) is acquired from Alfa Aesar. Fluorine-doped tin oxide (FTO: F:SnO_2) substrates are supplied by Pilkington. The indium zinc oxide (In_2O_3:ZnO, 85:15 wt%) target is purchased from Testbourne Ltd., UK.

Preparation of perovskite precursor

Perovskite 1:

The perovskite composition is $Rb_{0.05}Cs_{0.05}MA_{0.05}FA_{0.85}Pb(I_{0.95}Br_{0.05})_3$. The precursor solution is prepared by mixing FAI, MABr, $PbBr_2$, PbI_2, CsI and RbI in a molar ratio of 0.85, 0.05, 0.05, 0.95, 0.05 and 0.05 respectively in a 4:1 volume ratio of DMF: DMSO solvents, and the molar concentration is 1.5 M. A small amount of RbCl is also added into the precursor solution to mitigate the $J-V$ hysterisis.

Perovskite 2:

The perovskite composition is $Cs_{0.05}(MA_{0.17}FA_{0.83})_{0.95}Pb(I_{0.83}Br_{0.17})_3$. The perovskite precursor solution is prepared by dissolving 1.1 M PbI_2, 1 M FAI, 0.2 M MABr, and 0.22 M $PbBr_2$ in a 1 ml of DMF and DMSO mixture solution (4:1), followed by stirring for 2 hours. Subsequently, 52 µL of CsI from a 1.5 M CsI stock solution in DMSO is added to 1 mL of the perovskite solution, and the mixture is stirred for an additional hour.

Perovskite 3:

The perovskite composition is $Cs_{0.05}MA_{0.16}FA_{0.79}Pb(I_{0.67}Br_{0.33})_3$. The precursor solution is prepared by dissolving 1.12 M FAI, 0.21 M MABr, 0.64 M $PbBr_2$ and 0.85 M PbI_2 in 1 mL DMF and DMSO mixture (4:1) solution followed by the addition of 47 µL of CsI from a 1.5 M in DMSO stock solution.

Synthesis of Spiro-MeOTAD$^{\bullet+}$(TFSI$^-$)$_2$

In a 50 mL oven-dried flask, Spiro-MeOTAD (1.26 g, 1 mmol) and anhydrous dichloromethane (DCM) (20 mL) are added under continuous stirring in a nitrogen atmosphere. Silver(I) bis(trifluoromethanesulfonyl)imide (Ag-TFSI) (0.78 g, 2 mmol) is introduced gradually over 5 minutes at room temperature. The flask is then evacuated and refilled with nitrogen. The reaction mixture is stirred at room temperature for 24 hours. Following the reaction, the mixture is diluted by adding additional DCM. The resulting grey precipitate of silver (0) is removed by filtration using an Anopore inorganic membrane. The solvent from the filtrate is evaporated, yielding a dark solid. This solid is then dissolved in a minimal volume of DCM and subsequently precipitated in dry diethyl ether. The obtained fine, dark powder of Spiro-MeOTAD$_2^{\bullet+}$(TFSI$^-$)$_2$ is collected through filtration using an Anopore inorganic membrane. For crystallization, vapour diffusion of diethyl ether into a concentrated DCM solution of Spiro-MeOTAD$_2^{\bullet+}$(TFSI$^-$)$_2$ is performed at 8°C, resulting in the formation of dark crystals.

Synthesis of TBMP$^+$TFSI$^-$

To a 100 mL flask, tBP (1.35 g, 10 mmol) and anhydrous acetonitrile (10 mL) were added with stirring under a nitrogen atmosphere. Iodomethane (4.2 g, 30 mmol) in anhydrous acetonitrile (2.5 mL) was introduced using a dropping funnel over 30 minutes at room temperature. The resulting mixture was then heated under reflux for 16 hours and subsequently allowed to cool to room temperature. Following the removal of the solvent under reduced pressure, the crude product, 4-tert-butyl-1-methylpyridinium iodide (TBMP$^+$I$^-$), was obtained and further purified through recrystallization. Anion exchange processes were employed to obtain other TBMP$^-$ based salts. To a solution of TBMP$^+$I$^-$ (1.39 g, 5 mmol) in methanol (5 mL), a solution of silver(I) bis(trifluoromethanesulfonyl)imide (Ag-TFSI) (10 mmol) in acetonitrile (5 mL) was added dropwise to the heated reaction mixture under magnetic stirring. A dense yellow precipitate of silver(I) iodide formed. After refluxing for four hours, the precipitate was filtered off and rinsed with methanol. The solvent from the filtrate was then evaporated, yielding a waxy solid, 4-tert-butyl-1-methylpyridinium bis(trifluoromethanesulfonyl)imide (TBMP$^+$TFSI$^-$).

Transparent perovskite solar cells fabrication:

The perovskite solar cells (PSCs) are fabricated on commercially available fluorine-doped tin oxide (FTO) substrates (Pilkington, 15 Ω/sq). Proper cleaning of FTO substrates is a crucial step in achieving high-efficiency PSCs. Therefore, the FTO substrates are sequentially cleaned

using an ultrasonic cleaner in various solutions, including a soap solution, deionized (DI) water, acetone, and isopropanol (IPA), with each step lasting 15 minutes. The cleaned substrates are then placed in an oven at 120 ℃ for 60 minutes, followed by cooling to room temperature before commencing the device fabrication process. Prior to the deposition of the bilayer electron transport layer (ETL), consisting of planar SnO_2 (P-SnO_2) derived from tin(IV) chloride pentahydrate ($SnCl_4 \cdot 5H_2O$) and colloidal SnO_2 (C-SnO_2), the substrates undergo UV ozone treatment for 30 minutes. The planar SnO_2 layer is spin-coated at 2000 rpm for 30 seconds and subsequently annealed at 180 ℃ for 1 hour. After cooling to room temperature, the colloidal SnO_2 layer is deposited by spin-coating at 4000 rpm for 30 seconds, followed by annealing at 150 ℃ for 30 minutes. To enhance the adhesion of the perovskite layer to the SnO_2 surface, the SnO_2-coated substrates are subjected to an additional UV ozone treatment for 30 minutes.

Perovskite 1:

The perovskite precursor solution is then deposited onto the FTO/P-SnO_2/C-SnO_2 substrates via spin-coating at 5000 rpm for 50 seconds, with a acceleration speed of 1000 rpm. To facilitate initial crystallization and ensure uniform film formation, 200 μL of chlorobenzene is dynamically dispensed onto the spinning substrate 25 seconds before the completion of the second spin-coating step. The perovskite-coated substrates are subsequently annealed in a nitrogen-filled glovebox at 100 ℃ for 10 minutes.

Perovskite 2:

The perovskite precursor solution is then deposited onto the FTO/P-SnO_2/C-SnO_2 substrates via spin-coating at 2000 rpm for 10 seconds, followed by 6000 rpm for 30 seconds. To facilitate initial crystallization and ensure uniform film formation, 200 μL of chlorobenzene is dynamically dispensed onto the spinning substrate 15 seconds before the completion of the second spin-coating step. The perovskite-coated substrates are subsequently annealed in a nitrogen-filled glovebox at 100 ℃ for 50 minutes.

Perovskite 3:

The perovskite precursor solution is then deposited onto the FTO/P-SnO_2/C-SnO_2 substrates via spin-coating at 4000 rpm for 40 seconds, with a acceleration speed of 1000 rpm. To facilitate initial crystallization and ensure uniform film formation, 200 μL of chlorobenzene is dynamically dispensed onto the spinning substrate 15 seconds before the completion of the

second spin-coating step. The perovskite-coated substrates are subsequently annealed in a nitrogen-filled glovebox at 120 ℃ for 30 minutes.

The regular (control) spiro-OMeTAD precursor solution is prepared by dissolving 80 mg of spiro-OMeTAD, 40 µL of 4-tert-butylpyridine (tBP), and 24 µL of lithium bis(trifluoromethanesulfonyl)imide (Li-TFSI) solution (520 mg/mL in acetonitrile) in 1 mL of chlorobenzene. The precursor solution is stirred in a glovebox for 30 minutes before use. The spiro-OMeTAD films are then deposited onto the perovskite layer by spin-coating at 4000 rpm for 30 seconds.

For the preparation of ion-modulated Spiro-OMeTAD, the neutral Spiro-OMeTAD is initially dissolved in CB at a concentration of 90 mg/mL. Additionally, the oxidized Spiro-OMeTAD complex is dissolved in TCE at a concentration of 110 mg/mL. The TBMPTFSI salt is also dissolved in TCE at a concentration of 21.5 mg/mL.

Two distinct solutions are then prepared as follows:

Spiro 1: 93 µL of neutral Spiro-OMeTAD, 7 µL of oxidized Spiro-OMeTAD radicals, and 21 µL of TBMPTFSI solution.

Spiro 2: 93 µL of neutral Spiro-OMeTAD, 7 µL of oxidized Spiro-OMeTAD radicals, and 35 µL of TBMPTFSI solution.

By mixing these two solutions in varying proportions, the desired doping concentrations of TBMPTFSI are achieved. The film deposition is carried out using static spin-coating at different spin speeds, depending on the specific requirements.

Subsequently, a rear electrode comprising 300 nm of IZO followed by Ag busbars of 200 nm thick is deposited by RF sputtering and thermal evaporation respectively. A buffer layer of WO3 of 10 nm is also deposited between HTL and IZO *via* thermal evaporation. Finally, to minimize reflection losses from the top surface of the device, a 110 nm and 90 magnesium fluoride (MgF_2) anti-reflective coating (ARC) is deposited on top and bottom of the device respectively using thermal evaporation.

Characterizations

The structural properties of SnO_2/perovskite films are analyzed using an X-ray diffractometer (Rigaku SmartLab) with a Cu Kα radiation source ($\lambda \approx 1.54$ Å). The thickness of the perovskite thin film is measured using a Dektak-XT profilometer. The optical characteristics of the perovskite films are assessed using a PerkinElmer Lambda 950S UV-Vis-NIR spectrophotometer equipped with an integrating sphere. Transmittance (T) and reflectance (R)

measurements are conducted, and the absorptance (A) is determined using the formula A = 100 – T – R. The photovoltaic performance of the devices is evaluated by measuring the $J-V$ characteristics using a Keithley 2400 source meter and a solar simulator. The solar simulator (Newport LSH-7320) provides AM 1.5G illumination at an intensity of 100 mW/cm^2, and all $J-V$ measurements are conducted at 25 ℃ and 40% relative humidity. The calibration of the solar simulator is performed using a reference silicon cell provided by ABET, under one-sun illumination. Here, the active area of the perovskite and Si cells is 0.175 cm^2 and 330 cm^2, respectively. Steady-state output power measurements are carried out by biasing the device at its maximum power point (MPP), as determined from the corresponding $J-V$ curve. The steady-state current is recorded using a Keithley 2400 source meter, and the output power is calculated by multiplying the bias voltage with the measured current density. The steady-state power conversion efficiency is then derived. The external quantum efficiency (EQE) of single-junction solar cells is measured in an ambient air environment using a Zolix SCS10-X150 system. The active area of the solar cells is illuminated with focused, chopped monochromatic light beams. Steady-state photoluminescence (PL) spectra of all perovskite samples are recorded using an Ocean Optics spectrometer under vacuum conditions, at a base pressure of 10^{-5} mbar in a custom-made chamber, with an excitation wavelength of 490 nm. Macroscopic lifetime measurements are performed using the Time-Correlated Single Photon Counting (TCSPC) acquisition technique. A Horiba Delta Diode (628 nm) with a pulse width of 60 ps, externally triggered at a specific repetition rate, serves as the excitation source, delivering a fluence of 5.91/cm^2. The emitted light is detected using a hybrid picosecond photodetector (HPPD-870) with minimal dark counts. The Instrument Response Function (IRF) is recorded using a milk powder-dispersed solution in a cuvette, achieving a time resolution of approximately 150 ps. Kelvin probe force microscopy (KPFM) measurements are conducted using an Asylum/Oxford Instrument MFP-3D Origin. KPFM images are also captured in the dark using the same instrument in dual-pass mode under ambient conditions. The PLQY is measured using an integrating sphere coupled with optical fibre and Andor made ICCD spectrometer.

External quantum efficiency

We measured the external quantum efficiency (EQE) of our devices using a Zolix SCS10-X150. The solar cells are masked with a metal aperture to ensure the entire active area is illuminated by a tungsten halogen lamp. To determine the EQE, the device's photocurrent spectrum is divided by that of a calibrated Si reference cell with a known EQE. Each photocurrent spectrum is acquire over approximately 80 seconds under ambient conditions. The equivalent short-circuit current density under 1 sun irradiance is determine from the EQE measurements by calculating the overlap integral of the AM1.5 photon flux spectrum.

$$J_{SC} = \int_0^{\infty} \varphi_{AM}(\lambda) EQE\ (\lambda) d\lambda \quad \text{..... (1)}$$

where q is the elementary charge and λ is the wavelength.

Kelvin Probe Force Microscopy (KPFM)

The work function of a material is calculated using following equaqtion,

$$V_{CPD} = \frac{\phi_s - \phi_t}{e} \quad \text{..... (2)}$$

Where, ϕ_{tip} is work function of the probe (Here we have calibrated using Au sample), e is the elctronic charge and V_{CPD} is the contact potential difference.

Time-Correlated Single Photon Counting (TCSPC)

The TCSPC data fited with the given quardatic equation:

$$f(t) = A_1 e^{\frac{-t}{\tau_1}} + A_2 e^{\frac{-t}{\tau_2}} \quad \text{..... (3)}$$

Where τ_1 refers to short-lived PL emission contributing to trap-mediated recombination, and τ_2 represent the long-lived lifetime attributed to radiative recombination.

Average life time

$$t_{avg} = \sum_{i=1,2} \frac{\alpha_i \tau_i^2}{\tau_i} \quad \text{..... (4)}$$

Photoluminescence Quantum Yield (PLQY)

The PLQY is calculated using the following equation,

$$\eta_{PL} = \frac{E_3 - E_2\ (1-A)}{L_1 \cdot A} \quad \text{..... (5)}$$

Where E_2 and E_3 represent the emission of the samples under off and on axis with laser. L_1 represents the emission of the laser without a sample and A represents absorption.

Quasi Fermi Level Splitting (QFLS)

To calculate the quasi-fermi level splitting, we can use the Shockley-Queisser equation which links the radiative recombination density of free charges (J_{rad}) with the chemical potential per free electron-hole pair, given by (μ) or the QFLS in the active materials.[1,2]

$$J_{rad} = J_{0,rad} \exp \frac{\mu}{k_B T} \quad \text{.....} \quad (6)$$

Here, $J_{0,rad}$ is the radiative thermal recombination current density in the dark, k_B is the Boltzmann constant and T is the temperature. We note that equation 6 is a simplification of Würfel's generalised Plank law which is only valid for a QFLS that is a few $k_B T$ smaller than the bandgap $\mu < E_g - 3k_B T$.[1] If radiative recombination comes only from free charges, the radiative recombination current is identical to the photoluminescence yield times the elementary charge, that is $J_{rad} = \phi PL \cdot e$. Moreover, we can define the PLQY as the ratio of radiative to total recombination ($J_{R,tot}$), where the latter is identical to the generation current density, J_G under open circuit conditions, V_{OC}

$$\text{PLQY} = \frac{J_{rad}}{J_{R,tot}} = \frac{J_{rad}}{J_G} \quad \text{.....} \quad (7)$$

So we can go next calculate the QFLS formula with the equation –

$$\mu = k_B T \ln\left(\text{PLQY} \cdot \frac{J_G}{J_{0,rad}}\right) \quad \text{.....} \quad (8)$$

J_G is taken from the S-Q limit. $J_{0,rad}$ can be obtained by using the conventional formula as discussed in previous works,[3]

$$J_{0,rad} = \int \text{EQE}\, \phi_{BB}\, dE \quad \text{.....} \quad (9)$$

Where we have integrated external quantum efficiency (EQE) with the black body spectrum ϕ_{BB} at 300K over the energy. The black body spectrum can be calculated using this formula,

$$\phi_{BB}(\epsilon, T) = \frac{2\epsilon^2}{h^3 c^2} \cdot \frac{1}{\exp\left(\frac{\epsilon}{k_B T}\right) - 1} \quad \text{.....} \quad (10)$$

After using the equation 8 to calculate quasi fermi level splitting we obtain the following data as provided in table S1.

Table S1: Obtained QFLS energies, J_G and $J_{0,rad}$ values for different bandgap samples.

Perovskite	Sample	J_G(Am^{-2})	$J_{0,rad}$ (Am^{-2})	PLQY (%)	QFLS (eV)
Perovskite 3	Ion	218.53	1.227×10^{-20}	3.9	1.367
	Reg	218.53	2.909×10^{-21}	0.31	1.339
Perovskite 2	Ion	245.85	6.565×10^{-21}	0.46	1.331
	Reg	245.85	6.073×10^{-20}	0.55	1.278
Perovskite 1	Ion	281.95	8.29×10^{-20}	1.2	1.29
	Reg	281.95	1.179×10^{-19}	0.28	1.24

Note 1

The fitting of the TCSPC carrier lifetime is performed using the following equation,

$$\frac{\partial n}{\partial t} = G - k_1\, n - k_2(np - {n_i}^2) - C_{nT} - E_{nT} \quad \text{..... (11)}$$

$$\frac{\partial p}{\partial t} = G - k_1\, n - k_2(np - {n_i}^2) \quad \text{..... (12)}$$

$$\frac{\partial n_T}{\partial t} = C_{nT} - E_{nT} \quad \text{..... (13)}$$

Where, C_{nT} is the rate of electron capture to empty traps, E_{nT} is the rate of electron emission from filled traps, k_2 is the radiative recombination co-efficient, k_1 is the mid-bandgap recombination factor, and G is the Photogeneration rate.

The analytical VOC is estimated from the following equations,

$$J_{SC,control} = qk_{1,control} n_i w\, exp^{\frac{V_{OC,control}}{2v_t}} \quad \text{..... (14)}$$

$$J_{SC,Ion-Spiro} = qk_{1,Ion-Spiro} n_i w\, exp^{\frac{V_{OC,Ion-Spiro}}{2v_t}} \quad \text{.....(15)}$$

$$V_{OC,control} = 2v_t \ln \frac{J_{SC,Control}}{qk_{1,control} n_i w} \quad \text{.....(16)}$$

$$V_{OC,Ion-Sprio} = 2v_t \ln \frac{J_{SC,Ion-Spiro}}{qk_{1,Ion-Spiro} n_i w} \quad \text{.....(17)}$$

$$\Delta V_{OC} = 2v_t \left[\frac{J_{SC,Ion-Spiro} \times K_{1,Control}}{J_{SC,Control} \times K_{1,Ion-Spiro}}\right] \quad \text{.....(18)}$$

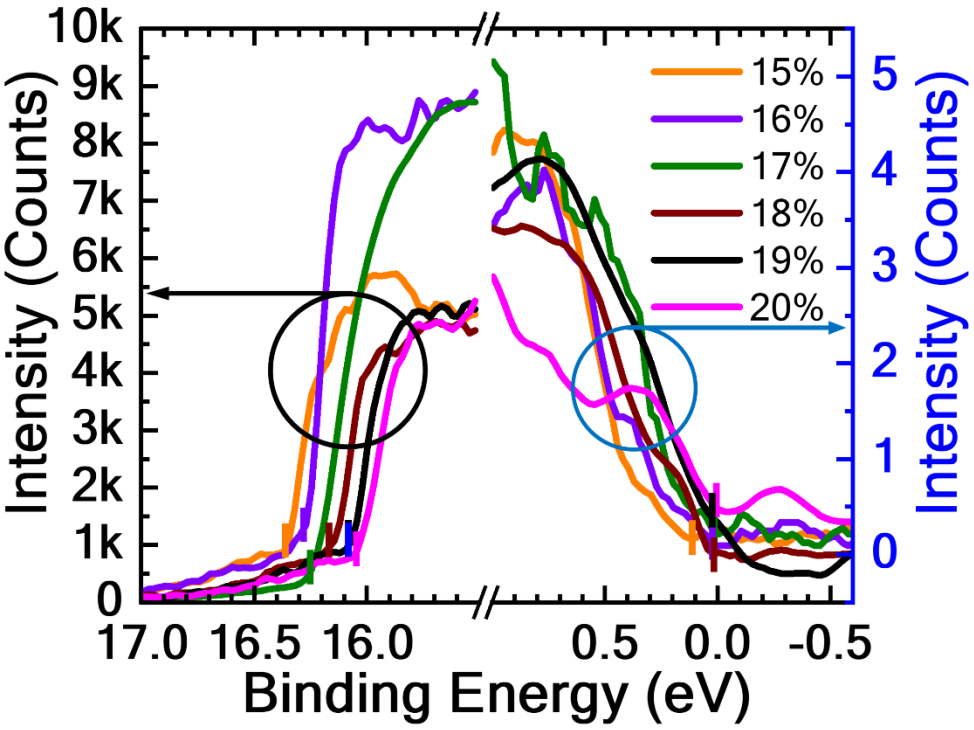

Figure S1: UPS spectra of varying TBMPTFSI salt concentration based Ion-Spiro MeOTAD HTLs.

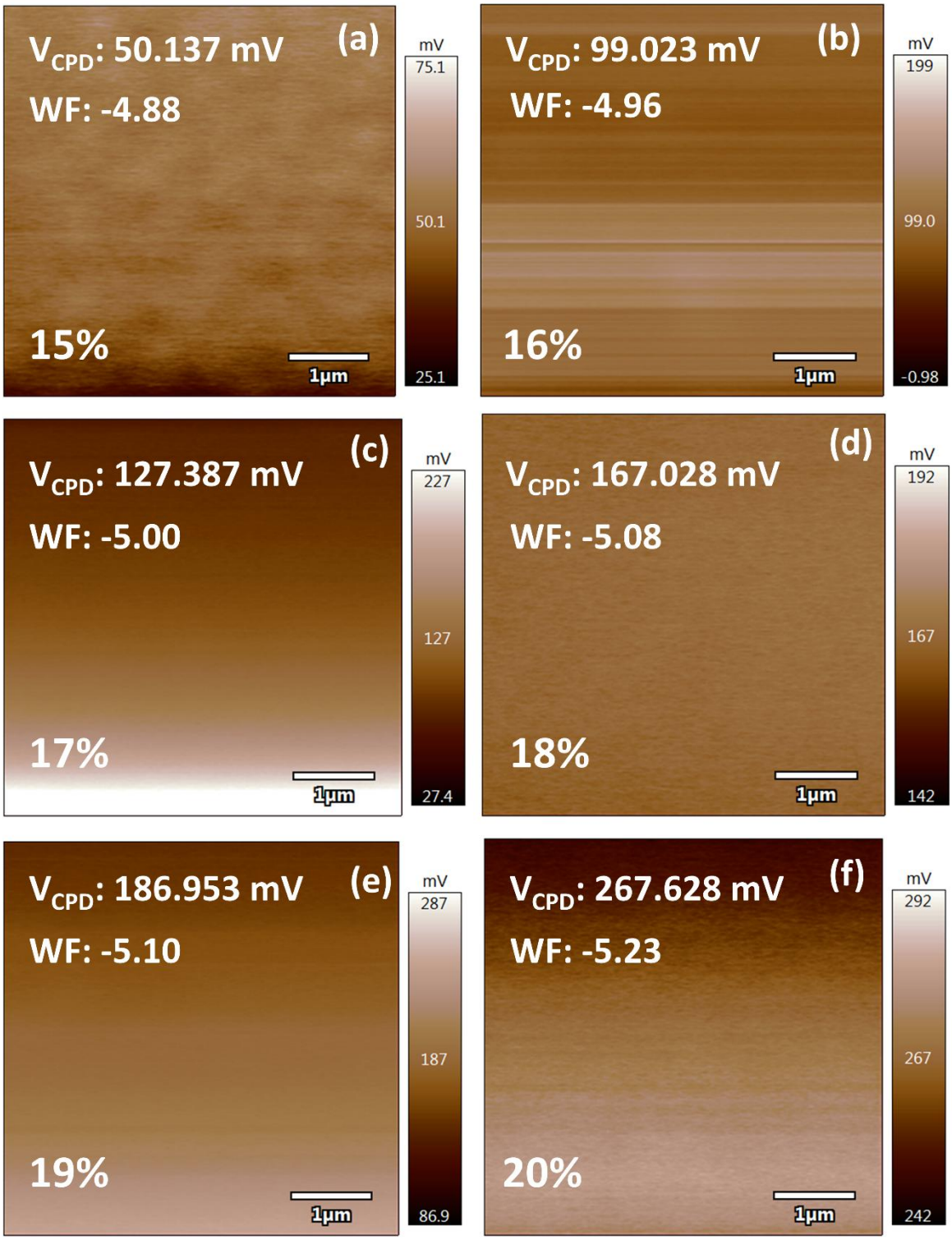

Figure S2: Work function (V_{CPD}) distribution of different TBMPTFSI doping concentration based Ion-modulated Spiro-MeOTAD thin films. A gradual increase of the V_{CPD} values with increase in doping concentration is observed which resulted in more deeper work function.

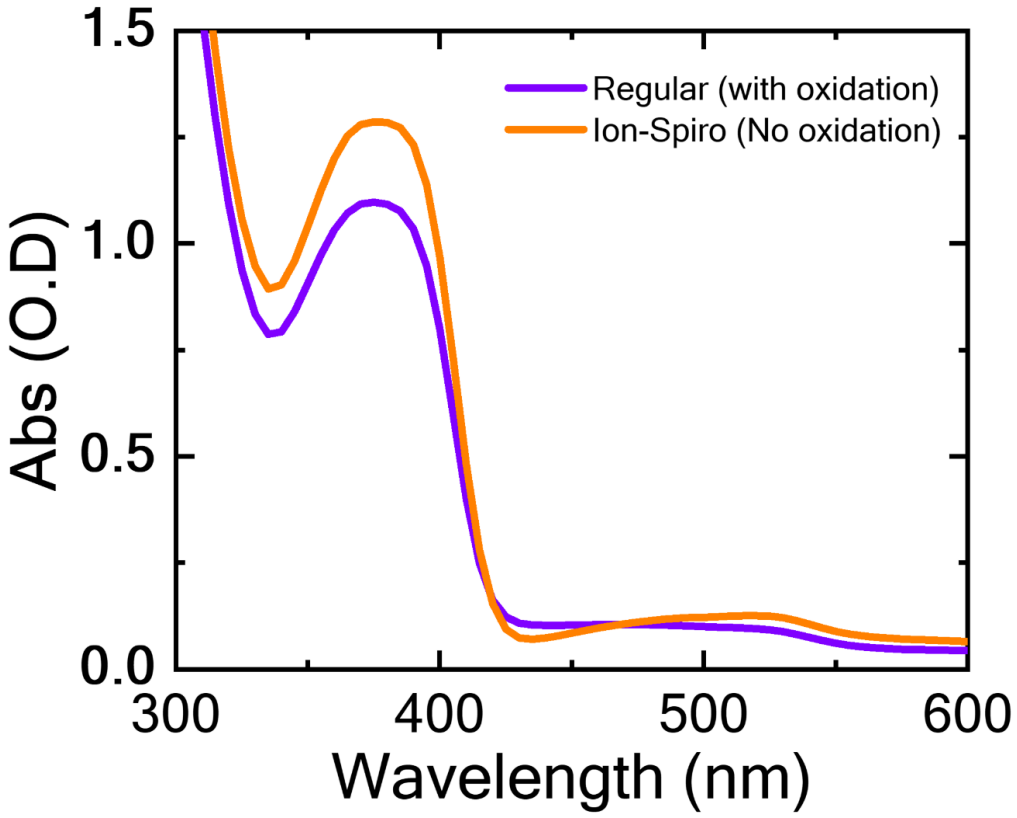

Figure S3: UV-Vis absorption analysis of oxidized regular Spiro-MeOTAD and non-oxidized Ion-modulated Spiro-MeOTAD. The absorption analysis confirms that similar optoelectronic properties are possessed by the Ion-modulated Spiro-MeOTAD without oxidation.

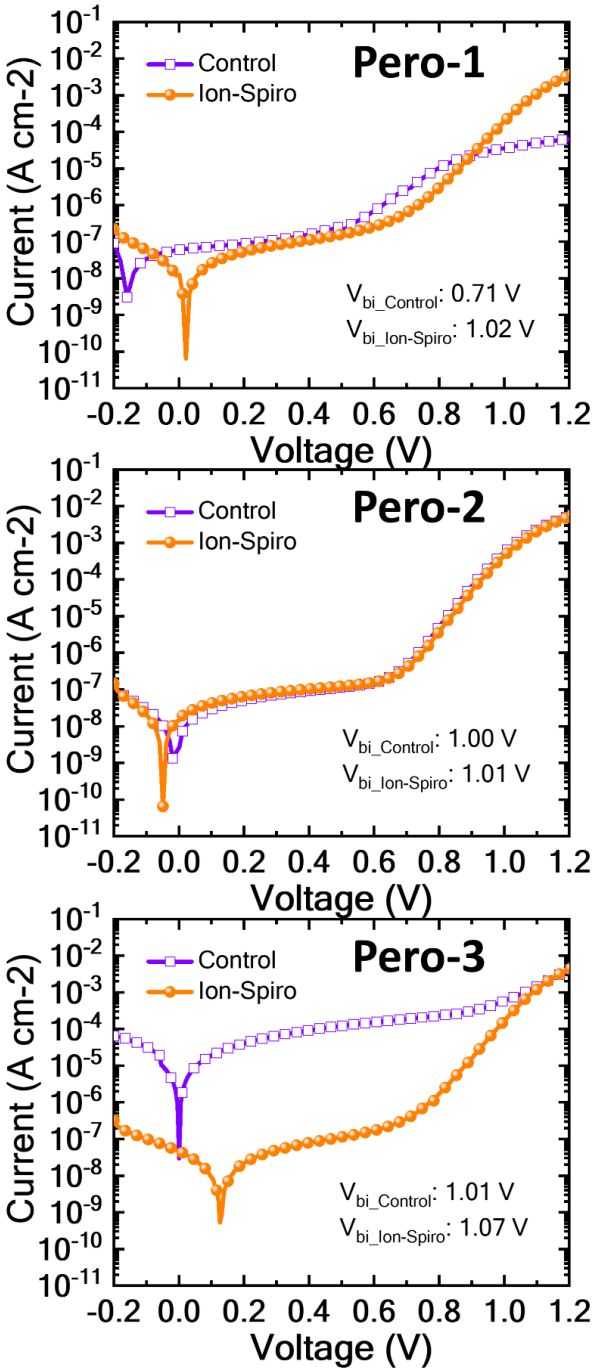

Figure S4: Dark $J-V$ characteristics of the control and Ion-Spiro HTL-based champion transparent PSCs. The built-in potential (V_{bi}) is consistently higher in the Ion-Spiro HTL-based devices, indicating the facilitation of a favourable energy band alignment and enhanced QFLS.

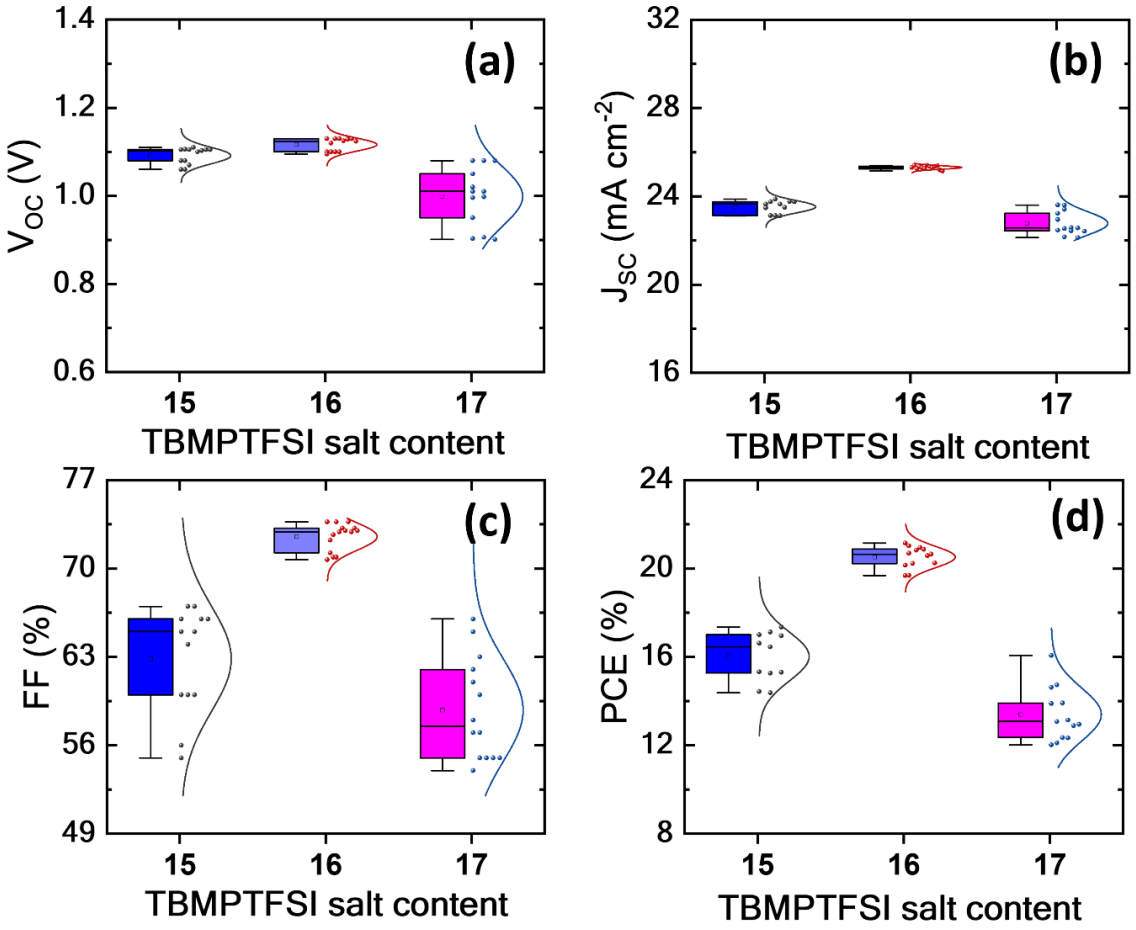

Figure S5: Variations of the PV performance of perovskite 1 with the TBMPTFSI doping concentrations. The 16% doping concentration is found to be optimal for perovskite 1.

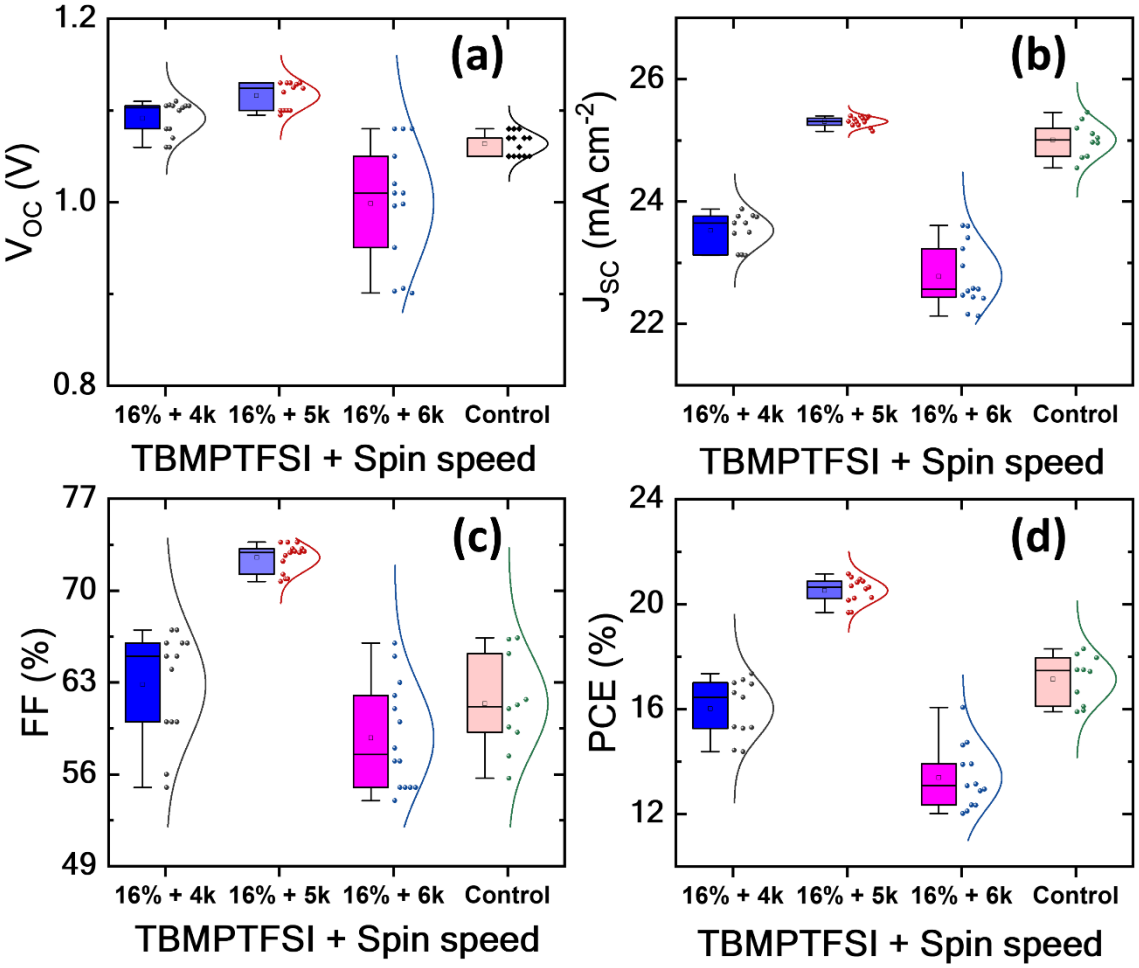

Figure S6: Variation of the PV performance of perovskite 1 with the spin speed, having optimal TBMPTFSI doping concentrations. The 5000 rpm of the spin speed is found to be optimal for perovskite 1.

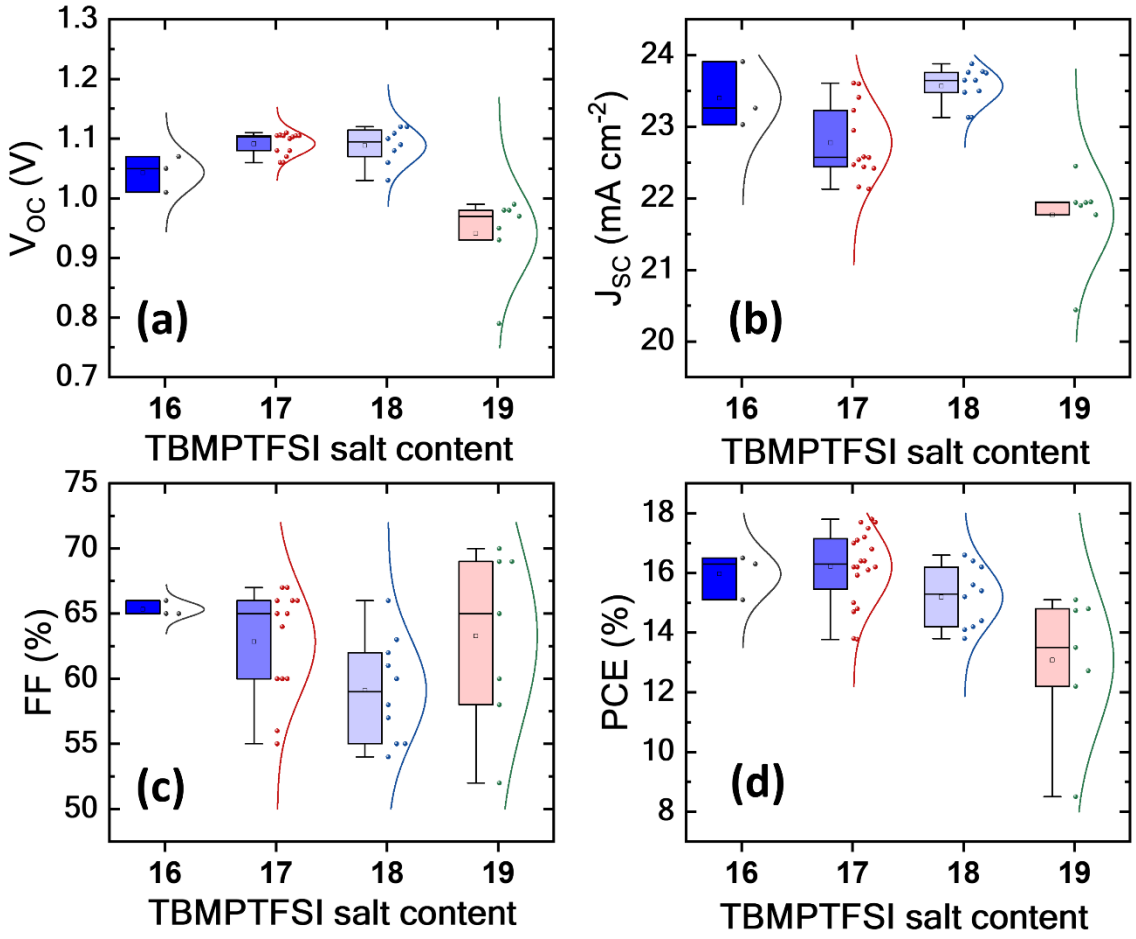

Figure S7: Variations of the PV performance of perovskite 2 with the TBMPTFSI doping concentrations. The 17% doping concentration is found to be optimal for perovskite 2.

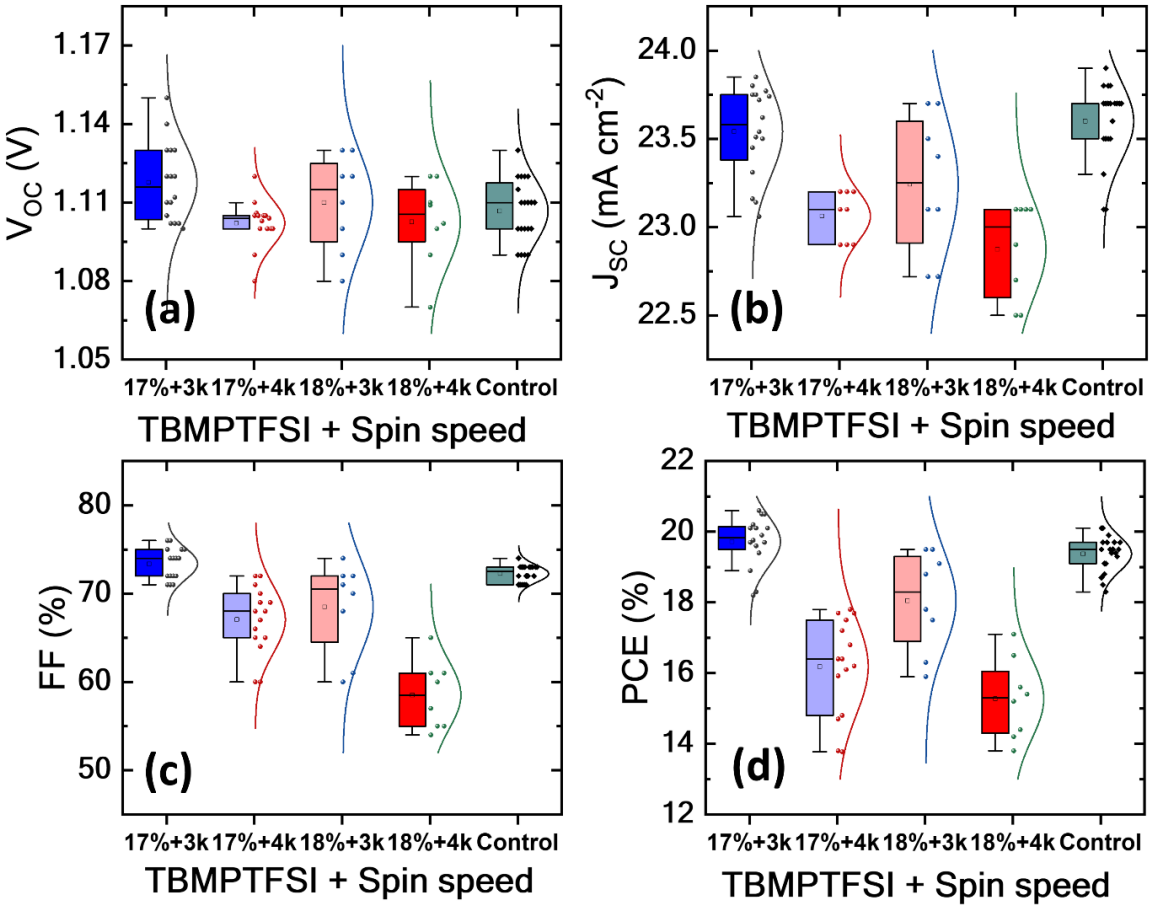

Figure S8: Variation of the PV performance of perovskite 2 with the spin speed, having 17% and 18% TBMPTFSI doping concentrations. The 3000 rpm of the spin speed with 17% doping is found to be optimal for perovskite 2.

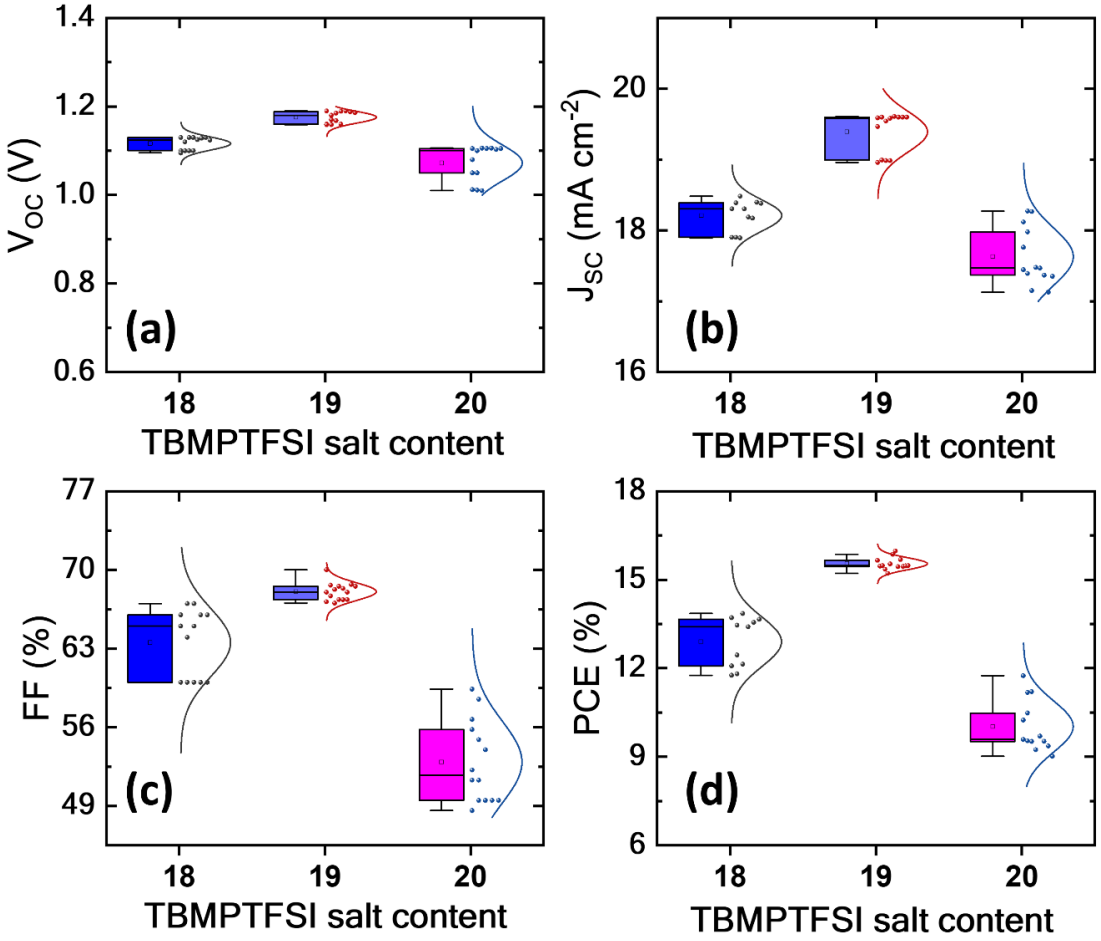

Figure S9: Variations of the PV performance of perovskite 3 with the TBMPTFSI doping concentrations. The 19% doping concentration is found to be optimal for perovskite 3.

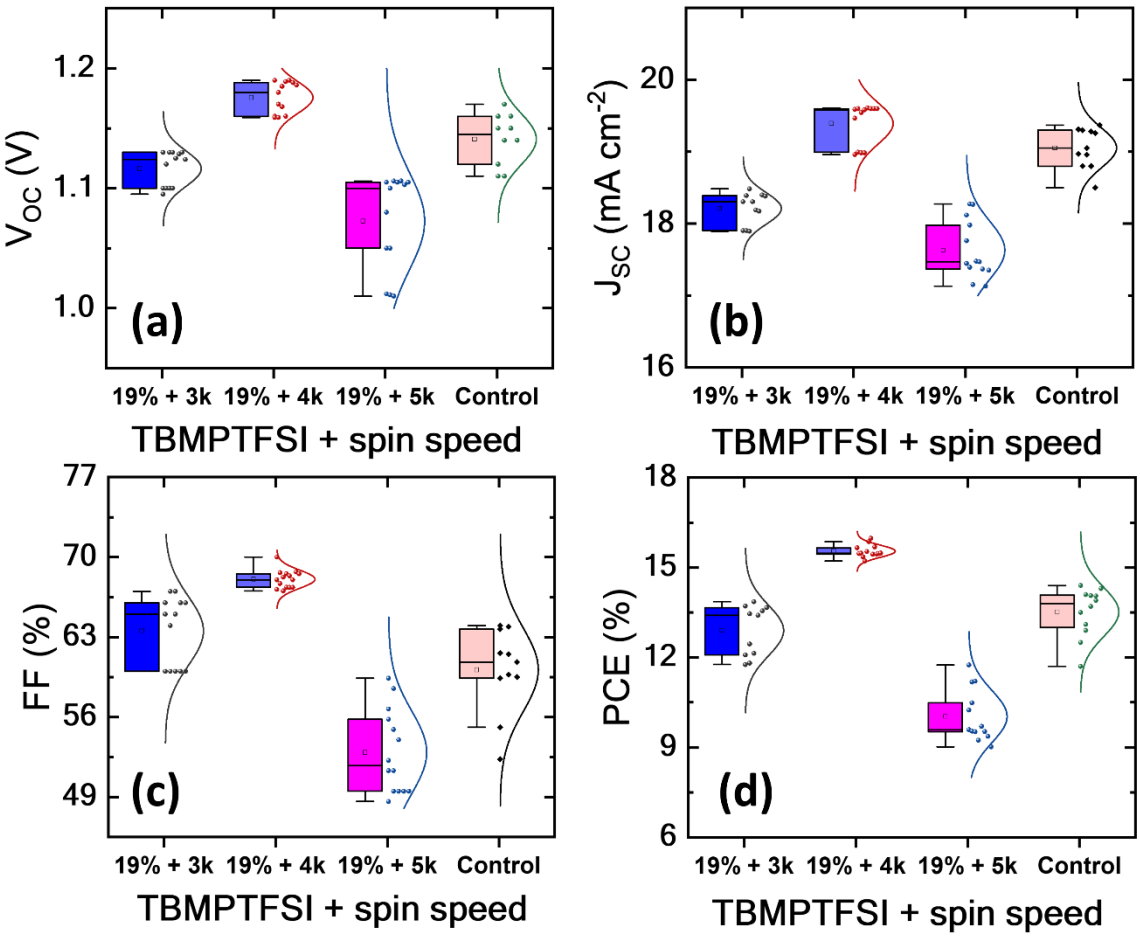

Figure S10: Variation of the PV performance of perovskite 3 with the spin speed, having optimal TBMPTFSI doping concentrations. The 4000 rpm of the spin speed is found to be optimal for perovskite 3.

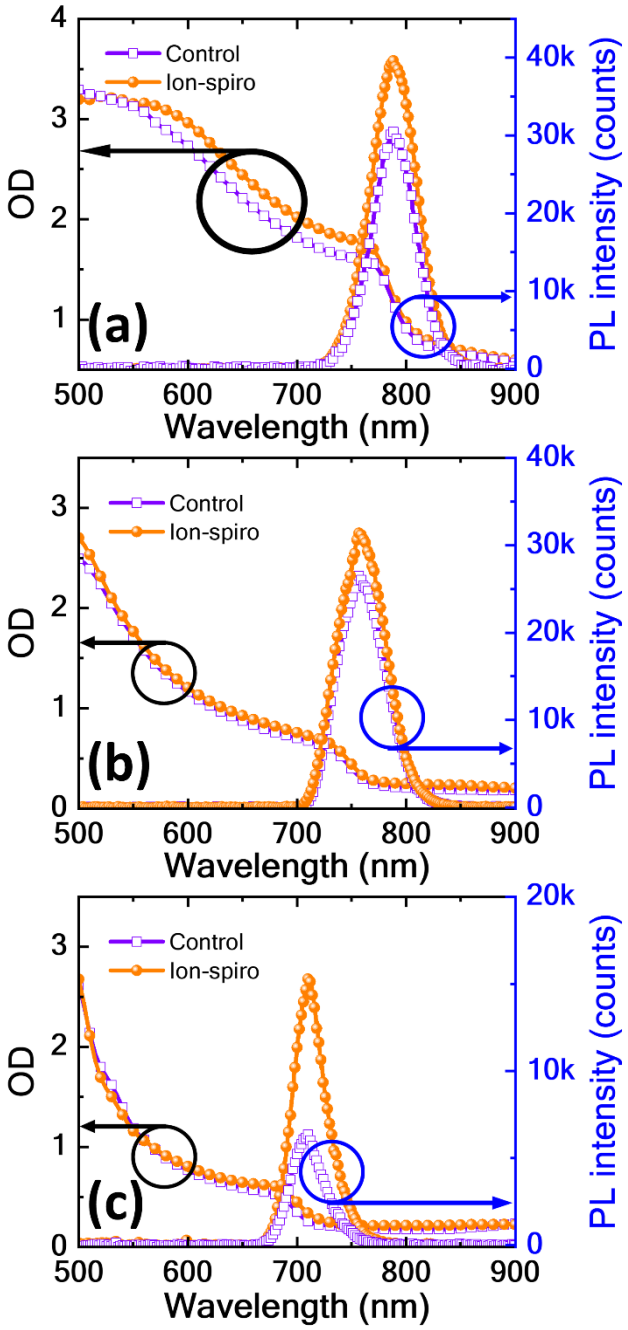

Figure S11: UV-Vis absorption and photoluminescence spectra of the bandgap varying transparent semi-processed PSCs (Glass/FTO/SnO_2/Perovskite 1, 2, and 3/Control or ion-spiro HTL) with control and Ion-modulated Spiro-MeOTAD HTL.

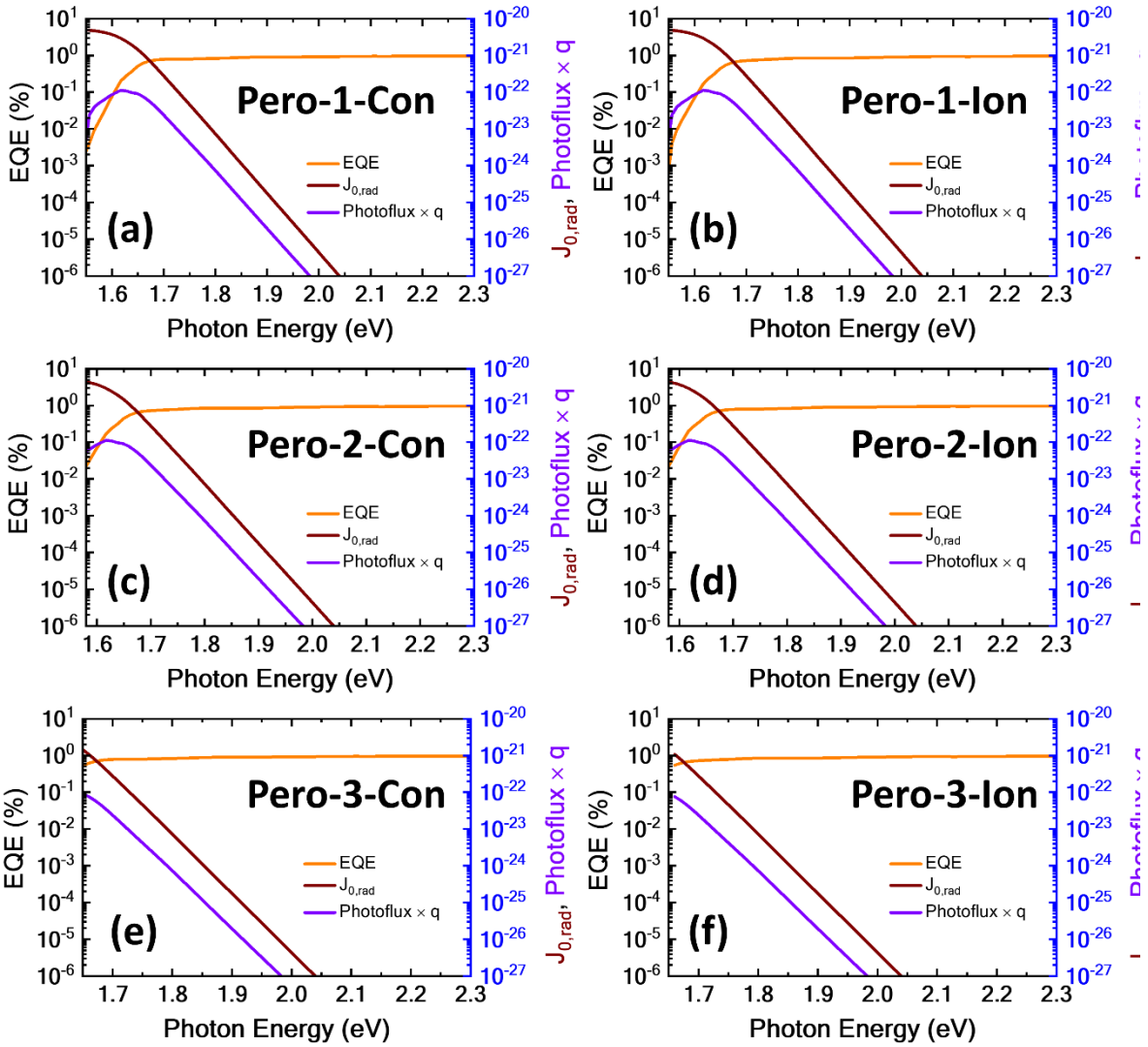

Figure S12: Photon Energy vs EQE, $J_{0,rad}$, photon flux for (a, c, and e) control and (b, d, and e) ion-modulated Spiro-MeoTAD HTL-based samples of (a, b) perovskite 1 (c, d) perovskite 2 (e, f) perovskite 3, respectively.

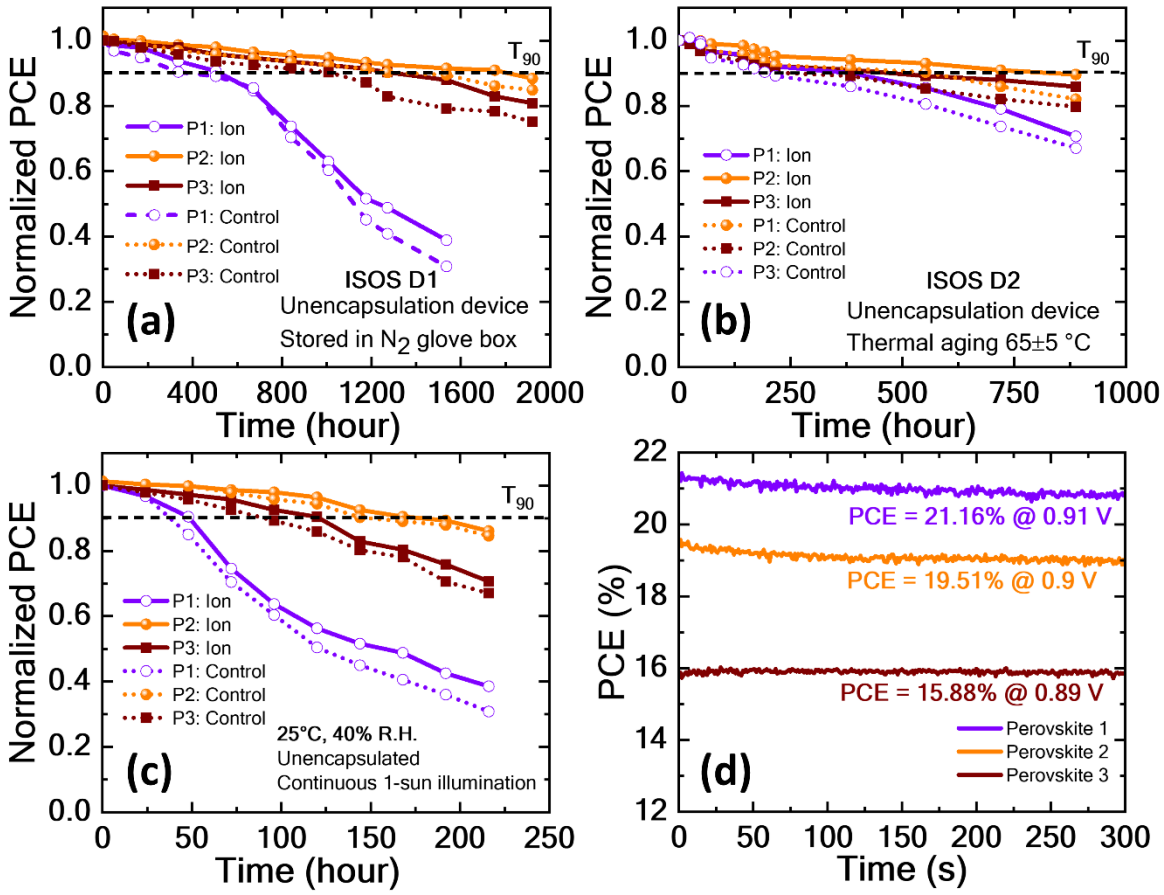

Figure S13: Stability analysis of the control and Ion-Spiro-based transparent PSCs under (a) dark storage in N_2, (b) continuous heating at 65 °C, (c) continuous 1 sun illumination, (d) maximum power point tracking (MPPT) storing conditions. It was observed that under all conditions the Ion-Spiro-based samples possess better stability for every perovskite composition.